Fringing analysis and forward modeling of Keck Planet Imager and Characterizer (KPIC) spectra

Katelyn A. Horstman, Jean-Baptiste Ruffio, Jason J. Wang, Chih-Chun Hsu, Ashley Baker, Luke Finnerty, Jerry Xuan, Daniel Echeverri, Dimitri Mawet, Geoffrey A. Blake, Randall Bartos, Charlotte Z. Bond, Benjamin Calvin, Sylvain Cetre, Jacques-Robert Delorme, Greg Doppmann, Michael P. Fitzgerald, Nemanja J. Jovanovic, Ronald Lopez, Emily C. Martin, Evan Morris, Jacklyn Pezzato, Garreth Ruane, Ben Sappey, Tobias Schofield, Andrew Skemer, Taylor Venenciano, J. Kent Wallace, Ji Wang, Peter Wizinowich

Published version information:

Citation: Katelyn A. Horstman et al., Proceedings Volume 13096, Ground-based and Airborne Instrumentation for Astronomy X; 130962E (2024)

DOI: https://doi.org/10.1117/12.3018020

Fringing analysis and forward modeling of Keck Planet Imager and Characterizer (KPIC) spectra

Katelyn A. Horstman[a,⋆], Jean-Baptiste Ruffio[b], Jason J. Wang[c], Chih-Chun Hsu[c], Ashley Baker[a], Luke Finnerty[d], Jerry Xuan[a], Daniel Echeverri[a], Dimitri Mawet[a,e], Geoffrey A. Blake[m], Randall Bartos[e], Charlotte Z. Bond[f], Benjamin Calvin[d], Sylvain Cetre[h], Jacques-Robert Delorme[h], Greg Doppmann[h], Michael P. Fitzgerald[h], Nemanja Jovanovic[a], Ronald Lopez[d], Emily C. Martin[i], Evan Morris[i], Jacklyn Pezzato[a], Garreth Ruane[a,e], Ben Sappey[b], Tobias Schofield[a], Andrew Skemer[i], Taylor Venenciano[k], J. Kent Wallace[e], Ji Wang[l], and Peter Wizinowich[h]

[a]Department of Astronomy, California Institute of Technology, Pasadena, CA 91125, USA
[b]Center for Astrophysics and Space Sciences, University of California, San Diego, La Jolla, CA 92093
[c]Center for Interdisciplinary Exploration and Research in Astrophysics (CIERA), Northwestern University, 1800 Sherman, Evanston, IL, 60201, USA
[d]Department of Physics & Astronomy, 430 Portola Plaza, University of California, Los Angeles, CA 90095, USA
[e]Jet Propulsion Laboratory, California Institute of Technology, 4800 Oak Grove Dr.,Pasadena, CA 91109, USA
[f]UK Astronomy Technology Centre, Royal Observatory, Edinburgh EH9 3HJ, United Kingdom
[g]Department of Astronomy, University of California at Berkeley, CA 94720, USA
[h]W. M. Keck Observatory, 65-1120 Mamalahoa Hwy, Kamuela, HI, USA
[i]Department of Astronomy & Astrophysics, University of California, Santa Cruz, CA 95064, USA
[j]Center for Astrophysics and Space Sciences, University of California, San Diego, La Jolla, CA 92093
[k]Physics and Astronomy Department, Pomona College, 333 N. College Way, Claremont, CA 91711, USA
[l]Department of Astronomy, The Ohio State University, 100 W 18th Ave, Columbus, OH 43210 USA
[m]Division of Geological & Planetary Sciences, California Institute of Technology, Pasadena, CA 91125, USA

ABSTRACT

The Keck Planet Imager and Characterizer (KPIC) combines high contrast imaging with high resolution spectroscopy (R∼35,000 in K band) to study directly imaged exoplanets and brown dwarfs in unprecedented detail. KPIC aims to spectrally characterize substellar companions through measurements of planetary radial velocities, spins, and atmospheric composition. Currently, the dominant source of systematic noise for KPIC is fringing, or oscillations in the spectrum as a function of wavelength. The fringing signal can dominate residuals by up to 10% of the continuum for high S/N exposures, preventing accurate wavelength calibration, retrieval of atmospheric parameters, and detection of planets with flux ratios less than 1% of the host star. To combat contamination from fringing, we first identify its three unique sources and adopt a physically informed model of Fabry-Pérot cavities to apply to post-processed data. We find this strategy can effectively model the fringing in observations

⋆NSF Graduate Research Fellow, Send correspondence to khorstma@astro.caltech.edu.

Ground-based and Airborne Instrumentation for Astronomy X, edited by Julia J. Bryant, Kentaro Motohara, Joël R. D. Vernet, Proc. of SPIE Vol. 13096, 130962E
 · 0277-786X · doi: 10.1117/12.3018020

of bright stars, reducing the residual systematics caused by fringing by a factor of 2. Next, we wedge two of the transmissive optics internal to KPIC to eliminate two sources of fringing and confirm the third source as the entrance window to the spectrograph. Finally, we apply our previous model of the Fabry-Pérot cavity to new data taken with the wedged optics to reduce the amplitude of the residuals by a factor of 10.

Keywords: exoplanets, instrumentation, high contrast imaging, high resolution spectroscopy, Keck telescope, fringing

1. INTRODUCTION

The goal of the Keck Planet Imager and Characterizer (KPIC) is to spectrally characterize exoplanets by measuring their radial velocities, spins, and atmospheric parameters. KPIC also seeks to develop key technologies to search for biosignatures, or signs of life, on potentially habitable planets outside our solar system. Achieving the photon noise limit for KPIC observations is difficult and requires an accurate model of the data that accounts for the spectra of the host star and companion, as well as characterizable systematics, such as atmospheric variability or optical fringing.

KPIC (R∼35,000)(1; 2) is a fiber fed, high contrast imaging instrument suite that interfaces with the high dispersion NIRSPEC echelle spectrograph on Keck 2 (3; 4). KPIC residuals show systematic fringing, or periodic oscillations in the continuum flux as a function of wavelength, visible within both NIRSPEC (5) and KPIC (6). This type of fringing is caused by transmissive optics or the detector itself acting as a Fabry-Pérot cavitiy within the instrument and is present in instruments such as the high-resolution iSHELL spectrograph ($R \sim 80,000$) (7) and in the Medium Resolution Spectrograph (MRS) of JWST/MIRI (8).

For high signal-to-noise (S/N) observations, the fringing amplitude can reach up to 10% of the stellar continuum in KPIC (6), overwhelming the photon noise for a typical observation. This poses problems for fitting stellar spectra used for deriving wavelength solutions, retrieving accurate elemental abundances in exoplanet atmospheres, and detecting faint planets as the fringing signal can overwhelm spectral features on the order of 1% the stellar continuum, especially if the fringing period is commensurate with spectral patterns in the target atmosphere. Several different attempts have been made to mitigate the fringing signatures. For temporal observations of Hot Jupiters, (9) removed the time-varying fringing signal attributed to the KPIC optics by using PCA analysis. For directly imaged companion observations, (10) incorporated a physics-based approach to model the contaminated residuals of their spectra to account for extra systematics, while (11; 12) applied a Fourier filter to remove the main frequencies associated with the periodic fringing signal. In this work, we explore another method to mitigate the fringing signal as well as alter physical optics to address the systematics outside of post-processing.

In section 2, we explain how several transmissive optics in KPIC/NIRSPEC act as Fabry-Pérot cavities and the properties of each unique optic related to the transmission of the fringing signal. In section 3, we create a physically informed model of Fabry-Pérot cavity to mitigate the fringing signal caused by each transmissive optic in KPIC/NIRSPEC. In section 4, we describe the application and results of applying the model of Fabry-Pérot cavities to on-sky observations. Finally, in section 5 we describe how we changed the physical optics themselves to remove the most difficult to characterize fringing signals and reapply our Fabry-Pérot cavity model to on-sky observations incorporating the new optics.

2. FABRY-PÉROT CAVITIES WITHIN KPIC/NIRSPEC

2.1 Fabry-Pérot cavities

Fabry-Pérot cavities are made of parallel interfaces with non-zero reflectivity and can create regular fringes from constructively and destructively interfering light (13). The transmittance of a single cavity is given by:

$$T = \frac{(1-R)^2}{1-2R\cos\delta + R^2} = \frac{1}{1+F\sin^2(\frac{\delta}{2})} \tag{1}$$

where R is the reflectance of the surface of the cavity, F is coefficient of finesse, and δ is the phase difference. The optical path length can be expressed as:

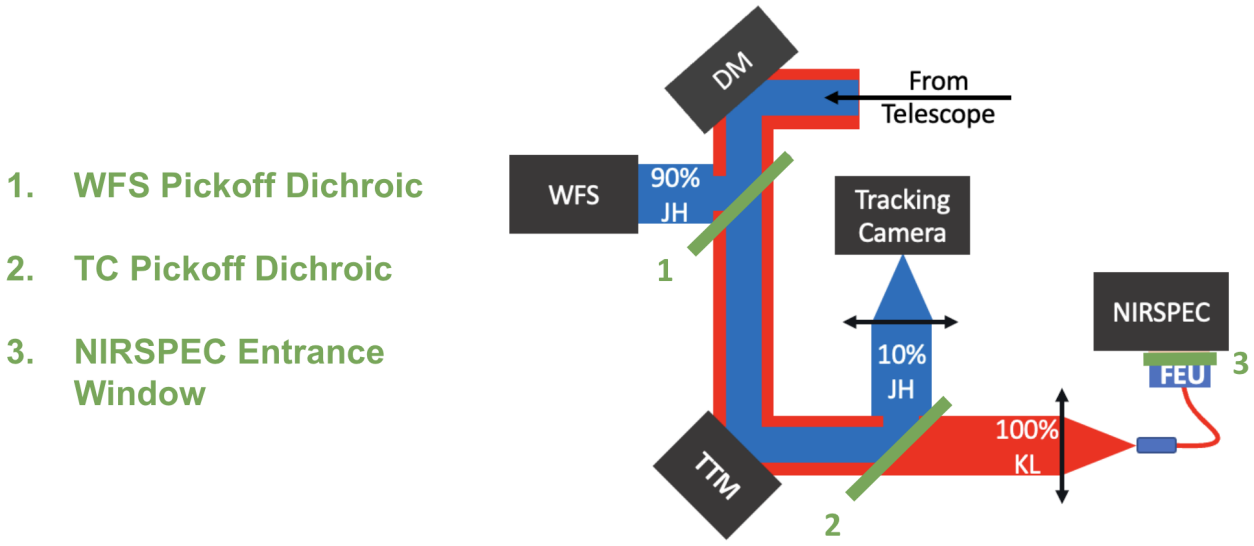

Figure 1: Optical path of KPIC/NIRSPEC. All transmissive optics are represented and labeled in the diagram in green. The following abbreviations are used: Deformable mirror (DM), wavefront sensor (WVS), tip-tilt mirror (TTM), fiber extraction unit (FEU), and tracking camera (TC). The properties of the transmissive optics are explained in subsection 2.2. Figure adapted from Figure 4a in (15).

$$\delta = \frac{2\pi}{\lambda} 2nl \cos\theta \tag{2}$$

where λ represents the wavelength of light, n, l are the index of refraction and thickness of the cavity, and θ is the angle of incidence (14). Therefore, the period only depends on the physical properties of the optic and wavelength of light propagating through the system.

However, in certain cases, transmissive optics can unintentionally act like Fabry-Pérot cavities. When the two surfaces of a transmissive optic are extremely parallel, they can form a Fabry-Pérot cavity, causing light to reflect back into its optical path. This happens when the coherence length of the light is larger than the size of the cavity, producing fringes or ghosts. Several transmissive optics used in KPIC and NIRSPEC can act as such cavities, as illustrated in Figure 1.

At 2 μm and with a refractive index of 1.5 at the resolution of KPIC, the coherence length is around 4 cm. Any unwedged optic thinner than this coherence length, could create a Fabry-Pérot cavity. subsection 2.2 describes the properties of the transmissive optics in KPIC/NIRSPEC that lead to exactly this behavior.

2.2 Properties of KPIC/NIRSPEC transmissive optics

NIRSPAO fringes have been well documented and are likely a result of the transmissive entrance window of NIRSPEC, impacting both NIRSPAO and KPIC/NIRSPEC data (5; 16; 17; 18; 19). However, these fringes are not as strong when the instrument is seeing-limited because of the low spatial coherence of the beam. The entrance window is made from calcium fluoride, which has a refractive index of 1.423 at 2 μm, is 7.5 mm thick, and is not coated in any additional material. The characteristics of the window are consistent with a 2Å feature induced by a Fabry-Pérot cavity, both in amplitude and period, when modeled using Equation 1.

Additionally, KPIC has with two identical dichroics that are transmissive in K and L band and reflective in J and H band. One dichroic is designed to send reflected light to a wavefront sensor and the other dichroic to send reflected light to a tracking camera, shown in Figure 1. Both dichroics are also constructed from calcium fluoride and are each 5 mm thick. These optics have a parallelism of less than 2.5″, which translates to approximately

5 mas on the sky when accounting for the beam compression factor. The theoretical reflectance of the entrance face is approximately 3.5%, while the reflectance of the exiting face is estimated to be 2.5% in K-band. Even though each dichroic has low finesse, it is sufficient to induce significant fringing since incoherent ghosting scales as R^2 instead of $2R$ for coherent light. The characteristics of each dichroic replicate a beating fringe pattern seen between 3-4 Å, where the period changes due to a changing optical path length caused by switching the fiber position during observations. Importantly, the identical dichroics create fringe patterns that *combine* with each other, causing high spatial and temporal variability of both the fringing amplitude and phase.

3. PHYSICALLY MOTIVATED FORWARD MODELING OF FABRY-PÉROT CAVITIES

Assuming the transmissive optics act as Fabry-Pérot cavities, we incorporate the physically motivated transmission, from Equation 1, into a forward model of on-sky observations. We model our KPIC observations of each target using the python package `breads`* (20), following the same methods used in (11; 12).

We define our forward model as,

$$\boldsymbol{d} = \boldsymbol{M}_{\mathrm{RV}}\boldsymbol{\phi} + \boldsymbol{n}, \tag{3}$$

where $\boldsymbol{d}$ is the data vector of size N_d, $\boldsymbol{M}_{\mathrm{RV}}$ represents the linear model, $\boldsymbol{\phi}$ represents the linear parameters, and $\boldsymbol{n}$ is a random vector of the noise with a diagonal covariance matrix $\boldsymbol{\Sigma}$, where $\boldsymbol{\Sigma} = \boldsymbol{\Sigma}_0 s^2$. $\boldsymbol{\Sigma}_0$ is defined using both the data vector and the standard deviation of the noise, and is multiplied by a free parameter scaling factor s^2 to account for any underestimation of the noise.

The non-linear parameters in our model include airmass and precipitable water vapor content at the observation site (W.M. Keck Observatory) to inform our telluric model, the radial velocity, $v \sin i$, effective temperature, $\log(g)$, and metallicity of the host to inform our stellar model, the amplitude of the stellar signal, and the number of nodes used in a 3$^{\mathrm{rd}}$ order spline model of the stellar continuum. We introduce eight additional parameters to account for the fringing based on the physical model of a Fabry-Pérot cavity:

$$T = \frac{1}{1 + F_0 \sin^2(\frac{a_0\lambda + b_0}{\lambda})} \times \frac{1}{1 + F_1 \sin^2(\frac{a_1\lambda + b_1}{\lambda})} \times \frac{1}{1 + F_1 \sin^2(\frac{a_2\lambda + b_2}{\lambda})} \tag{4}$$

where F is still the coefficient of finesse, but parameters a and b are used within a linear model to parameterize the phase. Since both dichroics have the same optical properties, we allow them to share a coefficient of finesse, which ultimately dictates the amplitude of the sinusoidal waves.

4. APPLICATION TO DATA

4.1 Data reduction

Spectra were reduced using the KPIC Data Reduction Pipeline (DRP) † following the same procedure as described in (21). In summary, the KPIC DRP performs background subtraction, bad pixel correction, and spectral trace calibration to determine the location and width of each of the nine NIRSPEC spectroscopic orders, orders 31-39, on the detector for each of KPIC's four fibers. In general, the most used KPIC order is $2.29 - 2.34\,\mu$m (order 33), which coincides with the CO bandhead. In our applications of the Fabry-Pérot cavity model, we focus on fitting order 33 as it is one of the easiest to fit that contains usable science content.

As part of the nightly KPIC calibrations, we take spectra of early M giant stars, which have narrow spectral lines due its slow rotation, to anchor and derive a wavelength solution for each spectroscopic order. The spectral lines from the M-calibrator star and telluric lines from the atmosphere are modeled with a PHOENIX model (22) and the Planetary Spectrum Generator (23), respectively, to obtain best fit parameters for the final wavelength solution in each order.

The difficulty of using this model lies in the fact that the fringe phase depends on the angle of incidence on the cavity. While it is believed that the NIRSPEC entrance window remains stable, the fringing caused by

*https://breads.readthedocs.io/en/latest/

†https://github.com/kpicteam/kpic_pipeline

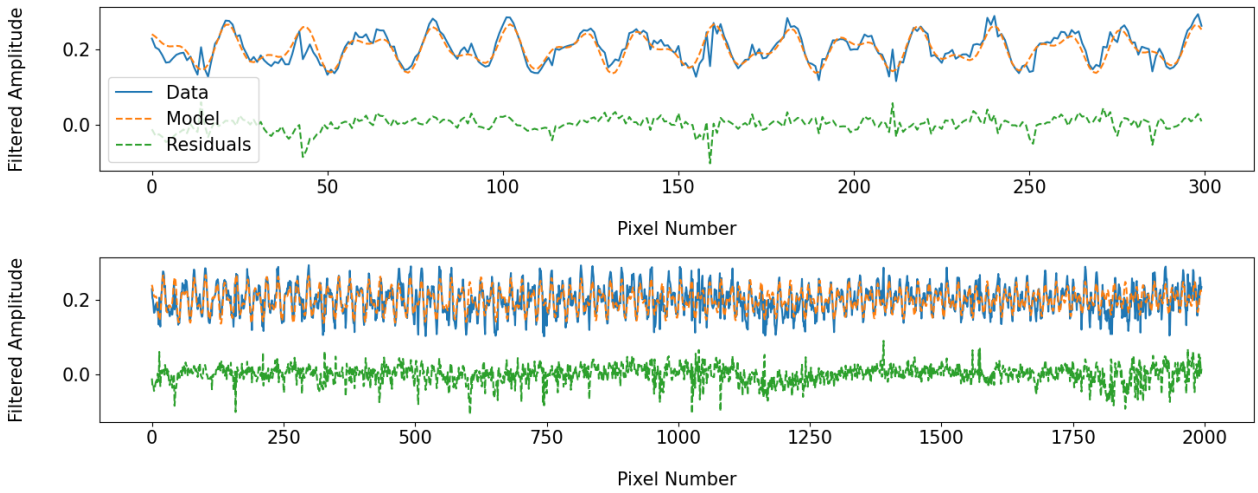

Figure 2: Normalized (data/model) fringing signal extracted from the A0 calibration star Zeta Aquilae in order 33 ($2.29 - 2.34\,\mu$m). **Top:** Zoomed in fringing signal fit to normalized stellar spectrum using Equation 4. The blue line depicts the data, while the model is in orange and the residuals are in green. **Bottom:** Same as top panel, except for the entire order. Best fit parameters can be found in Table 1.

	zet Aql	HR 8799	HIP 61960
F_0	5.3×10^{-2}	1.9×10^{-1}	6.3×10^{-1}
a_0	-5.0×10^{2}	-5.0×10^{2}	-1.1×10^{3}
b_0	6.8×10^{4}	6.8×10^{4}	6.9×10^{4}
F_1	1.5×10^{-1}	1.6×10^{-1}	NA
a_1	-5.4×10^{1}	5.8×10^{1}	NA
b_2	4.0×10^{4}	4.0×10^{4}	NA
a_1	-7.8×10^{1}	-7.4×10^{1}	NA
a_2	4.0	3.4	NA

Table 1: Best fit forward modelling parameters to Equation 4. The fit to Zeta Aquilae is to the normalized (data/model) fringing signal, while the fit to HR 8799 and HIP 61960 is to the stellar spectrum, with parameters corresponding to unwedged and wedged dichroics respectively.

the KPIC dichroics is highly variable since changing the fiber used for observation or offsetting to an off-axis companion changes the phase of the fringes. The distance between fibers, $0.8''$, roughly corresponds to one-third of a fringe wave. Consequently, developing a single model to account for fringing in every observation is difficult.

Thus, instead of developing a singular model for all observations, we create a framework for fitting a model to a variety of observations. First, we extract the fringes from a spectrum with few stellar or telluric lines by dividing our data by the best fit model for a A0V telluric calibration star. We fit our mathematical model, Equation 4, to the extracted empirical fringes to find values for each of the eight parameters. We implement a grid search over a space that is consistent with physical model parameters, matching in expected amplitude and phase, and check that the residuals are consistent with noise. We execute the grid search in several stages. First, we constrain the individual phases (a, b) for each dichroic separately, then we perform an additional search to constrain the two remaining amplitude terms (F_0, F_1). After using the grid search to find rough global parameters, we run a Nelder-Mead optimization to find the best fit parameters. Figure 2 shows the fringe extraction and fitting for an example A0V star, Zeta Aquilae while Table 1 shows the fitting results to each parameter.

4.2 Application to F0V host star

To test our model of observations on a host star, we again applied the fringing model to a spectrum with very few stellar lines to evaluate its performance with minimal noise sources. We applied the fringing parameters found

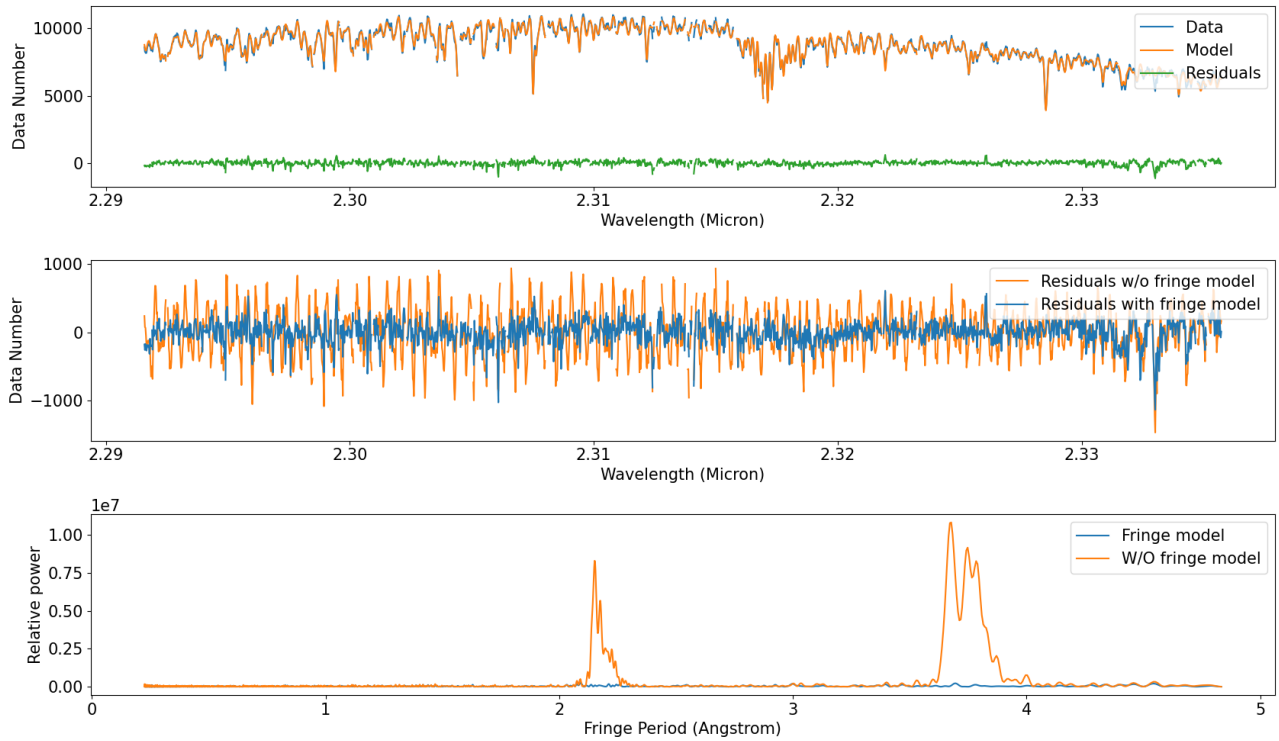

Figure 3: Example of forward modeling of the KPIC fringing signal, before wedging the dichroics, on a telluric calibrator star. **Top:** Spectrum of HR8799 after incorporating a fringing signal in the forward model framework. The data is in blue, the model is in orange, and the residuals (data-model) are in green. **Middle:** The residuals of the model including the fringing signal and the model not including the fringing signal. The residuals incorporating the fringing model are in blue, while the residuals that do not have any fringing mitigation are in orange. **Bottom:** A Lomb-scargle periodogram of the residuals of the model including the fringing signal and the model not including the fringing signal. The residuals incorporating the fringing model are in blue, while the residuals that do not have any fringing mitigation are in orange. The fringing signal due to transmissive optics within KPIC/NIRSPEC are clearly suppressed at 2Å and between 3-4 Å by the quantitative modeling framework, reducing the amplitude of the residuals by a factor of 2.

in Table 1 for Zeta Aquilae to an on-axis, bright star, HR 8799, as a best guess. We then ran a Nelder-Mead optimization to find the best fit parameters for our HR 8799 observation.

Figure 3 shows the fit of the forward model incorporating the fringing signal. The model was able to replicate the fringing pattern from all three sources, suppressing the fringing signal related to both the entrance window and dichroics, reducing the amplitude of the residuals by a factor of 2. The best fit parameters can be found in Table 1.

4.3 Application to M-giant wavelength calibration star

Next, we applied the fringing model to an M-giant star, primarily used for calibrating wavelength solution for each order in KPIC due to the star's deep, abundant stellar lines. Modeling the fringing signal for wavelength calibration stars is important for both obtaining a more precise wavelength solution and exploring whether the wavelength solution is biased by the fringes. Figure 4 shows the fit of the forward model incorporating the fringing signal.

We find that it is much more difficult to fit the spectrum of an M-giant star compared to bright, A0V/F0V stars because of mismatch between the stellar model and the data and the commensurate nature of the power spectrum of the fringing signal and the stellar lines. The amplitude of the residuals due to the mismatch is

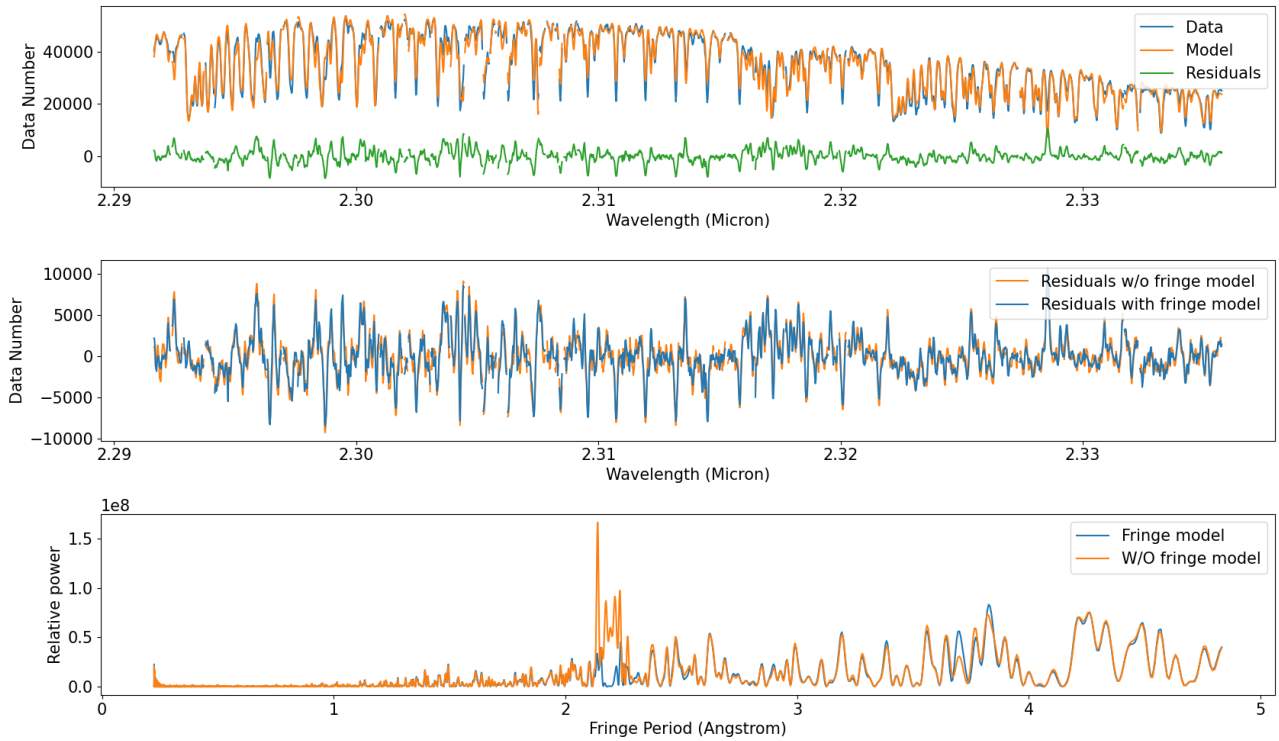

Figure 4: Example of forward modeling the KPIC fringing signal before wedging the dichroics on wavelength calibrator star. **Top:** Spectrum of HIP 95771 after incorporating a fringing signal in the forward model framework. The data is in blue, the model is in orange, and the residuals (data-model) are in green. There is mismatch between the depth of stellar lines in the model versus in the data. **Middle:** The residuals of the model including the fringing signal and the model not including the fringing signal. The residuals incorporating the fringing model are in blue, while the residuals that do not have any fringing mitigation are in orange. **Bottom:** A Lomb-scargle periodogram of the residuals of the model including the fringing signal and the model not including the fringing signal. The residuals incorporating the fringing model are in blue, while the residuals that do not have any fringing mitigation are in orange. Although the fringing signal appears to be slightly suppressed, the mismatch between the stellar lines of the model and data are on the same order of magnitude as the fringing signal. The power spectrum of the stellar atmosphere and that of the fringing signal have significant overlap, making it much more difficult to fit the fringes.

the same order of magnitude as the fringing residuals, making it difficult to avoid fitting model mismatch while fitting the fringing signal. No best fit parameters are reported because of this.

5. WEDGING DICHROICS TO REMOVE UNWANTED FRINGES

Since the parallelism of the dichroics creates several Fabry-Pérot cavities, we decided to modify the optics to alter the optical path of the fringing pattern, preventing it from re-entering the beam or falling on the detector. To combat the most difficult to parameterize and characterize fringing signals attributed to the dichroics, we introduced deviation by wedging the dichroics. We ordered new dichroics with a wedge angle of $50''$. At 2 μm, this results in approximately a 5 λ/D offset between the primary beam and the co-propagating ghost. The new dichroics were installed in April of 2024 as part of a KPIC service mission (24).

After wedging the dichroics in April of 2024, we confirm the presence of fringes due to the KPIC dichroics are no longer apparent. Figure 5 shows the Lomb-scargle periodogram of the residuals from our forward model fits for each KPIC fiber. As expected, we still observe the fringing signal at 2Å due the NIRSPEC entrance window, but no longer observe fringes between 3-4 Å due to the dichroics. We also verify that the dichroic fringing signal is no longer observed in different spectral orders or when offsetting to a companion.

5.0.1 Application to A0V calibration star after wedging dichroics

Since two of three sources of fringing are mitigated due to wedigng the dichroics, we once again apply our model in Equation 4 to on-sky observations with the new optics installed. However, since we now only see a single Fabry-Pérot cavity, we fit for 3 parameters instead of the original 8. Figure 6 shows the fit of the forward model incorporating the fringing signal while the best fit parameters can be found in Table 1.

From modeling the fringing, the signal is suppressed at the characteristic period of 2Å for the NIRSPEC entrance window and the amplitude of the residuals is reduced by a factor of 10, pushing KPIC observations closer to the photon noise limit than ever before. However, an additional signal is seen at 3-4 Å that is not apparent in Figure 5. This signal is not seen in Figure 5 and is difficult to notice except in analysis of residuals. The excess power between 3-4 Å could be do to leftover ghosts from the wedged dichroics, mismatch in the telluric model to the data, inaccurate flux extraction, or other currently unidentified systematics as explained in more detail in (25).

6. CONCLUSIONS AND FUTURE WORK

In this paper, we identify three unique sources of fringing, due to transmissive optics in KPIC/NIRSPEC and adopt a physically informed model of a Fabry-Pérot cavities to effectively model the fringing signal as seen in on-axis A0V/F0V stars. We adopt an instrumentation solution of wedging two of the transmissive optics internal to KPIC and verify the absence of the fringing signal due to the dichroics. By applying our fringing model to observations of A0V stars where the wedged dichroics are present, we find the fingring signal is suppressed at the characteristic period of 2Å for the NIRSPEC entrance window and the amplitude of the residuals is reduced by a factor of 10.

In the future, we need to verify that the NIRSPEC entrance window fringing signal is truly stable by looking at observations of the same star on different nights, across different fibers, between different orders, and on and off axis. Once we determine the entrance window is stable, we can probe whether a single physical model can be used to model all observations. Additionally, since there is only a single source of fringing after wedging the KPIC dichroics, which can be described by only three parameters, we plan to re-explore applying the forward model of the fringing to M-giant giant wavelength calibration stars to improve the wavelength solution of KPIC observations.

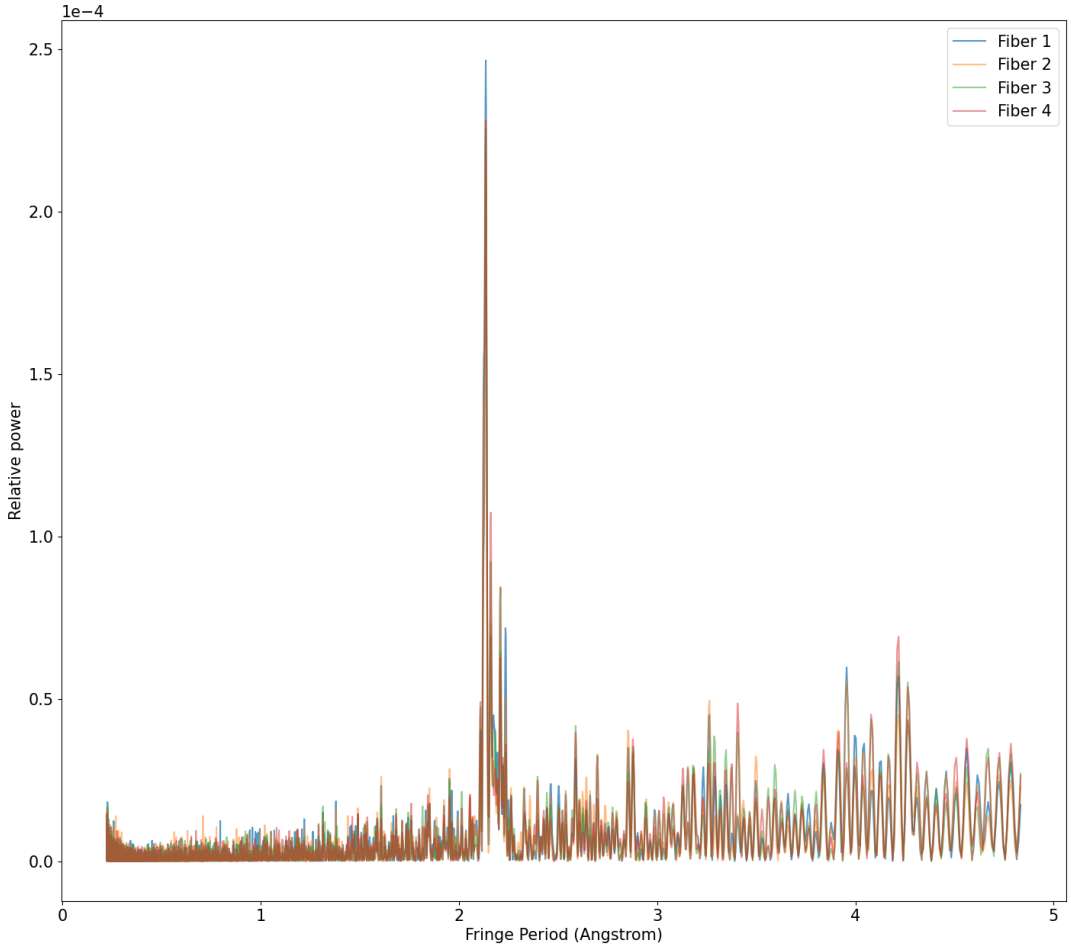

Figure 5: Lomb-scargle periodogram of the residuals (data-model) of HIP 61960 for each KPIC fiber. The fringing signal from the NIRSPEC entrance window at 2Å is present while the fringing signal from the dichroics between 3-4 Å is mitigated.

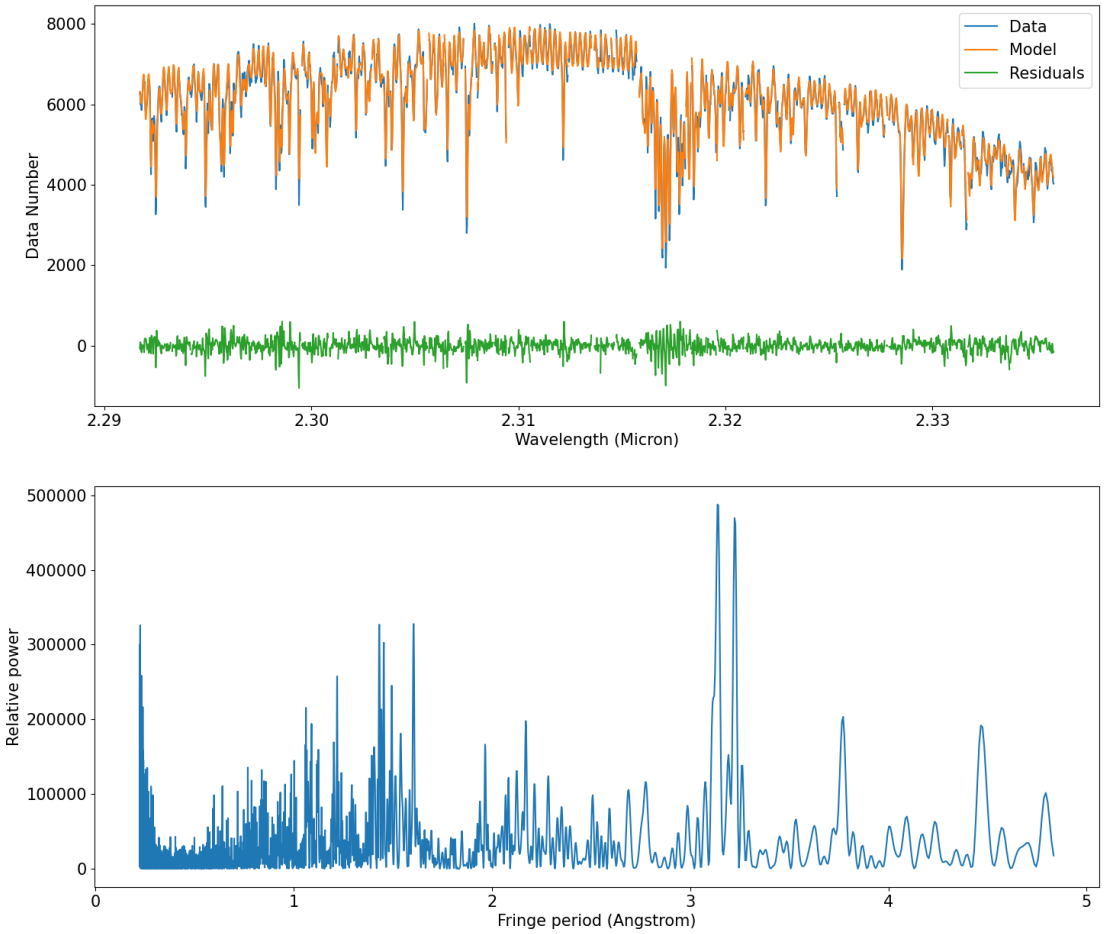

Figure 6: Example of forward modeling of the KPIC fringing signal, after wedging the dichroics, on a telluric calibrator star. **Top:** Spectrum of HIP 61960 after incorporating a fringing signal in the forward model framework. The data is in blue, the model is in orange, and the residuals (data-model) are in green. **Bottom:** A Lomb-scargle periodogram of the residuals of the model including the fringing signal. The incorporation of the the fringing model reduces the amplitude of the residuals by a factor of 10 compared to the model without the fringing model. The signal is suppressed for fringing due to the NIRSPEC entrance window at 2Å, but an additional signal is seen at 3-4 Å that is not apparent in Figure 5. The excess power between 3-4 Å could be do to leftover ghosts from the wedged dichroics, mismatch in the telluric model to the data, inaccurate flux extraction, or other currently unidentified systematics.

ACKNOWLEDGMENTS

K.H. is supported by the National Science Foundation Graduate Research Fellowship Program under Grant No. 2139433.

J.X. is supported by the NASA Future Investigators in NASA Earth and Space Science and Technology (FINESST) award #80NSSC23K1434.

Funding for KPIC has been provided by the California Institute of Technology, the Jet Propulsion Laboratory, the Heising-Simons Foundation (grants #2015-129, #2017-318, #2019-1312, #2023-4598), the Simons Foundation, and the NSF under grant AST-1611623.

The W. M. Keck Observatory is operated as a scientific partnership among the California Institute of Technology, the University of California, and NASA. The Keck Observatory was made possible by the generous financial support of the W. M. Keck Foundation. We also wish to recognize the very important cultural role and reverence that the summit of Maunakea has always had within the indigenous Hawaiian community. We are most fortunate to have the opportunity to conduct observations from this mountain. K.H. wishes to acknowledge her settler status on the ancestral lands of the Gabrielino/Tongva people and recognizes that the astronomical observations in this paper were possible because of the dispossession of Maunakea from the Kanāka Maoli.

References

[1] Mawet, D., Delorme, J. R., Jovanovic, N., Wallace, J. K., Bartos, R. D., Wizinowich, P. L., Fitzgerald, M., Lilley, S., Ruane, G., Wang, J., Klimovich, N., and Xin, Y., "A fiber injection unit for the Keck Planet Imager and Characterizer," in [*Society of Photo-Optical Instrumentation Engineers (SPIE) Conference Series*], Shaklan, S., ed., *Society of Photo-Optical Instrumentation Engineers (SPIE) Conference Series* **10400**, 1040029 (Sept. 2017).

[2] Delorme, J.-R., Jovanovic, N., Echeverri, D., Mawet, D., Kent Wallace, J., Bartos, R. D., Cetre, S., Wizinowich, P., Ragland, S., Lilley, S., Wetherell, E., Doppmann, G., Wang, J. J., Morris, E. C., Ruffio, J.-B., Martin, E. C., Fitzgerald, M. P., Ruane, G., Schofield, T., Suominen, N., Calvin, B., Wang, E., Magnone, K., Johnson, C., Sohn, J. M., López, R. A., Bond, C. Z., Pezzato, J., Sayson, J. L., Chun, M., and Skemer, A. J., "Keck Planet Imager and Characterizer: a dedicated single-mode fiber injection unit for high-resolution exoplanet spectroscopy," *Journal of Astronomical Telescopes, Instruments, and Systems* **7**, 035006 (July 2021).

[3] McLean, I. S., Becklin, E. E., Bendiksen, O., Brims, G., Canfield, J., Figer, D. F., Graham, J. R., Hare, J., Lacayanga, F., Larkin, J. E., Larson, S. B., Levenson, N., Magnone, N., Teplitz, H., and Wong, W., "Design and development of NIRSPEC: a near-infrared echelle spectrograph for the Keck II telescope," in [*Infrared Astronomical Instrumentation*], Fowler, A. M., ed., *Society of Photo-Optical Instrumentation Engineers (SPIE) Conference Series* **3354**, 566–578 (Aug. 1998).

[4] Martin, E. C., Fitzgerald, M. P., McLean, I. S., Doppmann, G., Kassis, M., Aliado, T., Canfield, J., Johnson, C., Kress, E., Lanclos, K., Magnone, K., Sohn, J. M., Wang, E., and Weiss, J., "An overview of the NIRSPEC upgrade for the Keck II telescope," in [*Ground-based and Airborne Instrumentation for Astronomy VII*], Evans, C. J., Simard, L., and Takami, H., eds., *Society of Photo-Optical Instrumentation Engineers (SPIE) Conference Series* **10702**, 107020A (Aug. 2018).

[5] Hsu, C.-C., Burgasser, A. J., Theissen, C. A., Gelino, C. R., Birky, J. L., Diamant, S. J. M., Bardalez Gagliuffi, D. C., Aganze, C., Blake, C. H., and Faherty, J. K., "The Brown Dwarf Kinematics Project (BDKP). V. Radial and Rotational Velocities of T Dwarfs from Keck/NIRSPEC High-resolution Spectroscopy," **257**, 45 (Dec. 2021).

[6] Finnerty, L., Schofield, T., Delorme, J.-R., Sappey, B., Wang, J. J., Ruffio, J.-B., Mawet, D., Fitzgerald, M. P., Jovanovic, N., Baker, A., Bartos, R., Bond, C., Bryan, M. L., Calvin, B., Cetre, S., Doppmann, G., Echeverri, D., Lopez, R., Martin, E., Morris, E., Pezzato, J., Ragland, S., Ruane, G., Skemer, A., Venenciano, T., Wallace, J. K., Wang, J., Wizinowich, P., and Xuan, J., "On-sky performance and lessons

learned from the phase I KPIC fiber injection unit," in [*Ground-based and Airborne Instrumentation for Astronomy IX*], Evans, C. J., Bryant, J. J., and Motohara, K., eds., **12184**, 121844Y, International Society for Optics and Photonics, SPIE (2022).

[7] Cale, B., Plavchan, P., LeBrun, D., Gagné, J., Gao, P., Tanner, A., Beichman, C., Xuesong Wang, S., Gaidos, E., Teske, J., Ciardi, D., Vasisht, G., Kane, S. R., and von Braun, K., "Precise Radial Velocities of Cool Low-mass Stars with iSHELL," **158**, 170 (Nov. 2019).

[8] Gasman, D., Argyriou, I., Sloan, G. C., Aringer, B., Álvarez-Márquez, J., Fox, O., Glasse, A., Glauser, A., Jones, O. C., Justtanont, K., Kavanagh, P. J., Klaassen, P., Labiano, A., Larson, K., Law, D. R., Mueller, M., Nayak, O., Noriega-Crespo, A., Patapis, P., Royer, P., and Vandenbussche, B., "JWST MIRI/MRS in-flight absolute flux calibration and tailored fringe correction for unresolved sources," **673**, A102 (May 2023).

[9] Finnerty, L., Schofield, T., Sappey, B., Xuan, J. W., Ruffio, J.-B., Wang, J. J., Delorme, J.-R., Blake, G. A., Buzard, C., Fitzgerald, M. P., Baker, A., Bartos, R., Bond, C. Z., Calvin, B., Cetre, S., Doppmann, G., Echeverri, D., Jovanovic, N., Liberman, J., López, R. A., Martin, E. C., Mawet, D., Morris, E., Pezzato, J., Phillips, C. L., Ragland, S., Skemer, A., Venenciano, T., Wallace, J. K., Wallack, N. L., Wang, J., and Wizinowich, P., "Keck Planet Imager and Characterizer Emission Spectroscopy of WASP-33b," **166**, 31 (July 2023).

[10] Xuan, J. W., Wang, J., Finnerty, L., Horstman, K., Grimm, S., Peck, A. E., Nielsen, E., Knutson, H. A., Mawet, D., Isaacson, H., Howard, A. W., Liu, M. C., Walker, S., Phillips, M. W., Blake, G. A., Ruffio, J.-B., Zhang, Y., Inglis, J., Wallack, N. L., Sanghi, A., Gonzales, E. J., Dai, F., Baker, A., Bartos, R., Bond, C. Z., Bryan, M. L., Calvin, B., Cetre, S., Delorme, J.-R., Doppmann, G., Echeverri, D., Fitzgerald, M. P., Jovanovic, N., Liberman, J., López, R. A., Martin, E. C., Morris, E., Pezzato, J., Ruane, G., Sappey, B., Schofield, T., Skemer, A., Venenciano, T., Wallace, J. K., Wang, J., Wizinowich, P., Xin, Y., Agrawal, S., Do Ó, C. R., Hsu, C.-C., and Phillips, C. L., "Validation of Elemental and Isotopic Abundances in Late-M Spectral Types with the Benchmark HIP 55507 AB System," **962**, 10 (Feb. 2024).

[11] Ruffio, J.-B., Horstman, K., Mawet, D., Rosenthal, L. J., Batygin, K., Wang, J. J., Millar-Blanchaer, M., Wang, J., Fulton, B. J., Konopacky, Q. M., Agrawal, S., Hirsch, L. A., Howard, A. W., Blunt, S., Nielsen, E., Baker, A., Bartos, R., Bond, C. Z., Calvin, B., Cetre, S., Delorme, J.-R., Doppmann, G., Echeverri, D., Finnerty, L., Fitzgerald, M. P., Jovanovic, N., López, R., Martin, E. C., Morris, E., Pezzato, J., Ruane, G., Sappey, B., Schofield, T., Skemer, A., Venenciano, T., Wallace, J. K., Wallack, N. L., Wizinowich, P., and Xuan, J. W., "Detecting Exomoons from Radial Velocity Measurements of Self-luminous Planets: Application to Observations of HR 7672 B and Future Prospects," **165**, 113 (Mar. 2023).

[12] Horstman et al. , "Rv measurements of directly imaged brown dwarf gq lup b to search for exo-satellites," (submitted).

[13] Perot, A. and Fabry, C., "On the Application of Interference Phenomena to the Solution of Various Problems of Spectroscopy and Metrology," **9**, 87 (Feb. 1899).

[14] Lipson, S. G., Lipson, H., and Tannhauser, D. S., [*Optical Physics*] (1995).

[15] Echeverri, D., Ruane, G., Jovanovic, N., Hayama, T., Delorme, J.-R., Pezzato, J., Bond, C., Wang, J., Mawet, D., Wallace, J. K., and Serabyn, E., "The vortex fiber nulling mode of the Keck Planet Imager and Characterizer (KPIC)," in [*Society of Photo-Optical Instrumentation Engineers (SPIE) Conference Series*], *Society of Photo-Optical Instrumentation Engineers (SPIE) Conference Series* **11117**, 111170V (Sept. 2019).

[16] Brown, T. M., Libbrecht, K. G., and Charbonneau, D., "A Search for CO Absorption in the Transmission Spectrum of HD 209458b," **114**, 826–832 (Aug. 2002).

[17] Deming, D., Brown, T. M., Charbonneau, D., Harrington, J., and Richardson, L. J., "A New Search for Carbon Monoxide Absorption in the Transmission Spectrum of the Extrasolar Planet HD 209458b," **622**, 1149–1159 (Apr. 2005).

[18] Blake, C. H., Charbonneau, D., and White, R. J., "The NIRSPEC Ultracool Dwarf Radial Velocity Survey," **723**, 684–706 (Nov. 2010).

[19] Theissen, C. A., Konopacky, Q. M., Lu, J. R., Kim, D., Zhang, S. Y., Hsu, C.-C., Chu, L., and Wei, L., "The 3D Kinematics of the Orion Nebula Cluster: NIRSPEC-AO Radial Velocities of the Core Population," **926**, 141 (Feb. 2022).

[20] Agrawal, S., Ruffio, J.-B., Konopacky, Q. M., Macintosh, B., Mawet, D., Nielsen, E. L., Hoch, K. K. W., Liu, M. C., Barman, T. S., Thompson, W., Greenbaum, A. Z., Marois, C., and Patience, J., "Detecting Exoplanets Closer to Stars with Moderate Spectral Resolution Integral-field Spectroscopy," **166**, 15 (July 2023).

[21] Wang, J. J., Ruffio, J.-B., Morris, E., Delorme, J.-R., Jovanovic, N., Pezzato, J., Echeverri, D., Finnerty, L., Hood, C., Zanazzi, J. J., Bryan, M. L., Bond, C. Z., Cetre, S., Martin, E. C., Mawet, D., Skemer, A., Baker, A., Xuan, J. W., Wallace, J. K., Wang, J., Bartos, R., Blake, G. A., Boden, A., Buzard, C., Calvin, B., Chun, M., Doppmann, G., Dupuy, T. J., Duchêne, G., Feng, Y. K., Fitzgerald, M. P., Fortney, J., Freedman, R. S., Knutson, H., Konopacky, Q., Lilley, S., Liu, M. C., Lopez, R., Lupu, R., Marley, M. S., Meshkat, T., Miles, B., Millar-Blanchaer, M., Ragland, S., Roy, A., Ruane, G., Sappey, B., Schofield, T., Weiss, L., Wetherell, E., Wizinowich, P., and Ygouf, M., "Detection and Bulk Properties of the HR 8799 Planets with High-resolution Spectroscopy," **162**, 148 (Oct. 2021).

[22] Husser, T. O., Wende-von Berg, S., Dreizler, S., Homeier, D., Reiners, A., Barman, T., and Hauschildt, P. H., "A new extensive library of PHOENIX stellar atmospheres and synthetic spectra," **553**, A6 (May 2013).

[23] Villanueva, G. L., Smith, M. D., Protopapa, S., Faggi, S., and Mandell, A. M., "Planetary Spectrum Generator: An accurate online radiative transfer suite for atmospheres, comets, small bodies and exoplanets," **217**, 86–104 (Sept. 2018).

[24] Echeverri, D. and KPIC Team, "Recent upgrades to the keck planet imager and characterizer," in [*SPIE Astronomical Telescopes + Instrumentation*], (2024).

[25] Wang, J. J., Mawet, D., Xuan, J. W., Hsu, C.-C., Ruffio, J.-B., Horstman, K., Xin, Y., Delorme, J.-R., Jovanovic, N., Zhang, Y., Finnerty, L., and KPIC Team, "The high-contrast performance of the keck planet imager and characterizer," in [*SPIE Astronomical Telescopes + Instrumentation*], (2024).